Separation Science and Technology
Publication details, including instructions for authors and subscription information:
http://www.informaworld.com/smpp/title~content=t713708471

Direct Contact Membrane Distillation of Sugar Aqueous Solutions

M. A. Izquierdo-Gil[a]; M. C. García-Payo[a]; C. Fernández-Pineda[a]
[a] DEPARTAMENTO DE FISICA APLICADA (TERMOLOGÍA), FACULTAD DE CIENCIAS FISICAS, UNIVERSIDAD COMPLUTENSE, MADRID, SPAIN

Online publication date: 22 June 1999

To cite this Article Izquierdo-Gil, M. A. , García-Payo, M. C. and Fernández-Pineda, C.(1999) 'Direct Contact Membrane Distillation of Sugar Aqueous Solutions', Separation Science and Technology, 34: 9, 1773 — 1801
To link to this Article: DOI: 10.1081/SS-100100738
URL: http://dx.doi.org/10.1081/SS-100100738

SEPARATION SCIENCE AND TECHNOLOGY, **34**(9), pp. 1773–1801, 1999

Direct Contact Membrane Distillation of Sugar Aqueous Solutions

M. A. IZQUIERDO-GIL,* M. C. GARCÍA-PAYO,†
and C. FERNÁNDEZ-PINEDA‡
DEPARTAMENTO DE FISICA APLICADA (TERMOLOGÍA)
FACULTAD DE CIENCIAS FISICAS
UNIVERSIDAD COMPLUTENSE
28040 MADRID, SPAIN

ABSTRACT

Results are given from direct contact membrane distillation, using tangential flows to the membrane, with sugar aqueous solutions. Several effects on the distillation process are examined: flow rate through the cell, nature of the feed solutions, initial concentrations of the feed solutions, average temperature, and temperature difference. On the basis of enthalpy flux conservation in the different regions, various systems of equations are proposed for the estimation of the interfacial temperatures. Based on the known temperatures of the liquid–vapor interfaces, the experimental distillate fluxes for several sets are fitted to the gas stagnant film diffusion model to obtain the effective diffusion coefficients of the water vapor–air mixture, D_{ef}, and the results are analyzed.

Key Words. Membrane distillation; Porous hydrophobic membrane; Direct contact; Temperature polarization; Gas stagnant film diffusion model

INTRODUCTION

Membrane distillation (MD) is a process of separation through hydrophobic porous membranes driven by a temperature difference. In direct contact

* To whom correspondence should be addressed. FAX: 34-913944643. E-mail: amparo@eucmax.sim.ucm.es
† E-mail: mcgpayo@eucmos.sim.ucm.es
‡ E-mail: fdezpine@eucmos.sim.ucm.es

membrane distillation (DCMD), the subject of this paper, hot temperature aqueous solution (feed) is brought into contact with one side of the membrane and cold distilled water (permeate) into contact with the other, so that the water vapor pressure is different at each side of the membrane. This pressure difference drives the water vapor through the membrane pores, and then the vapor condenses in contact with the distilled water on the other side. This process is commercially interesting in widely different fields: desalination, separation of volatile and nonvolatile solutes, and the concentration of liquid foods such as milk, fruit juices, etc. It offers the advantage of working at atmospheric pressure and room temperature, and the possibility of using geothermal, wave, or solar energy, or low temperature gradients available in industrial plants.

The hydrophobic nature of the membrane prevents the penetration of liquid water into the pores unless a higher pressure than the so-called liquid entry pressure of water (LEPw) is applied. Liquid vapor menisci are formed at the pore entrances, and these menisci act as liquid–vapor interfaces. The main requirement in this process is that the membrane should not be wetted, thus the pores must be small enough to prevent liquid penetration through the membrane under MD operating conditions. Their typical pore sizes must range from 100 Å to 1 μm, the surface tension of the liquid must be high, and the surface energy of the membrane must be low.

Most published studies have dealt with the effect of various parameters on the transport phenomenon: the applied temperature difference, the average temperature, the temperature polarization in the different systems, and the flow rate through the cell. In the case of solutions other than pure liquids, other parameters have been studied, such as the concentration difference, the average concentration, etc. (1–4). This paper presents a systematic study of the effect on membrane distillation, using tangential flows to the membrane, of the following parameters: the flow rate through the cell, the nature of the feed solution, the initial concentration of the feed, the average temperature, and the temperature difference. Equations have been developed to estimate the liquid–vapor interface temperatures. The experimental distillate fluxes are fitted to the equation of the gas stagnant film diffusion model.

THEORY

Temperature Polarization Models

Temperatures measured in bulk solutions in contact with a membrane are not the same as those in the liquid–vapor interface which are not accessible experimentally. A method had to be found to estimate these from the measurable bulk temperatures. This was done from enthalpy flux conservation.

The total enthalpy flux is made up of the conduction heat flux and the enthalpy flux due to diffusion (5). Thus, by solving the implied second-order differential equation which satisfies the conditions $T = T_1$ for $y = 0$, and $T = T_2$ for $y = y_1$, the temperature profile in this case is:

$$T = T_1 + \frac{T_1 - T_2}{1 - \exp[C_0^* y_1/k]} (\exp[C_0^* y/k] - 1) \tag{1}$$

where k is the thermal conductivity, T is the temperature, y is the variable along which the enthalpy is transferred, and $C_0^* = Nc_p$, with N the mass flux density and c_p the specific heat at constant pressure. The following function is often called the "Ackermann correction" for mass transfer (5):

$$\frac{\frac{C_0^* y_1}{k}}{\exp[C_0^* y_1/k] - 1}$$

If the heat flux by conduction is obtained from Eq. (1) for $y = 0$, then by a second-order approximation and adding the enthalpy flux accompanying mass transfer, the total enthalpy flux assumes a simple form in that limit (6):

$$\lim_{N \to 0} q_{H-I} = h_1 (T_1 - T_2) + Nc_p \left(\frac{1}{2} (T_1 + T_2) - T_0 \right) \tag{2}$$

where h_1 is the heat transfer coefficient which may be written as k_1/y_1, T_0 is the reference temperature, and the other quantities have already been defined.

The enthalpy flux in the other regions can be calculated in the same way (Fig. 1) by considering the phase transition enthalpies where ever they occur. Thus the following equations are obtained:

$$\begin{aligned} h_1 (T_1 - T_2) + Nc_{pL} \left(\frac{T_1 + T_2}{2} - T_0 \right) \\ = N \left[c_{pL} (T_2 - T_0) + \Delta H_v (T_2) + \frac{1}{2} c_{pv} (T_3 - T_2) \right] + \frac{k_m}{\delta} (T_2 - T_3) \end{aligned} \tag{3}$$

$$\begin{aligned} h_1 (T_1 - T_2) + Nc_{pL} \left(\frac{T_1 + T_2}{2} - T_0 \right) \\ = h_2 (T_3 - T_4) + Nc_{pL} \left(\frac{T_3 + T_4}{2} - T_0 \right) \end{aligned}$$

where h_1 and h_2 are the heat transfer coefficients from the feed bulk solution to the membrane surface and from the other membrane surface to the bulk solution on the distillation side, respectively; T_1, T_2, T_3, and T_4 are the temperatures in the feed bulk solution, at the hot surface of the membrane, on the other

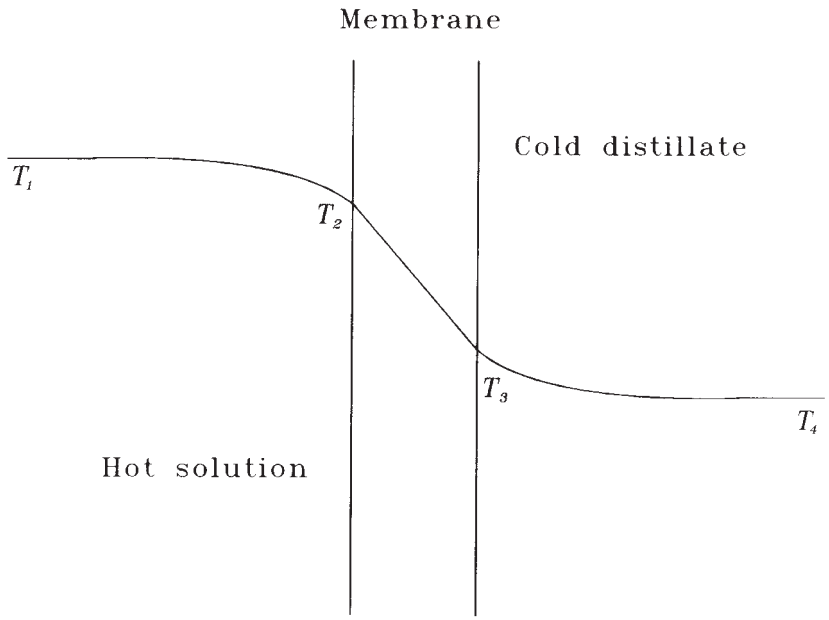

FIG. 1 Temperature profile in membrane distillation.

membrane surface, and in the cold bulk solution, respectively; C_{pL} and C_{pV} are the specific heats at constant pressure of the distillate in the liquid and in the gas phases, respectively; N (kg/m^2·s) is the mass flux density; $\Delta H_v(T_2)$ is the water evaporation enthalpy at temperature T_2; δ is the membrane thickness; and k_m is the thermal conductivity of the membrane, which may be expressed as

$$k_m = \varepsilon k_{gas} + (1 - \varepsilon) k_{matrix} \tag{4}$$

where ε is the void volume fraction, and k_{gas} and k_{matrix} are the thermal conductivities of the gases in the pores and of the membrane matrix, respectively.

By using Eqs. (3) together with the known heat transfer coefficients, the temperatures in the liquid–vapor interfaces of the membrane can be estimated.

Under our experimental conditions and in the most unfavorable case, the terms of $Nc_p\Delta T$ are, at most, of the order of 7% of the terms $N\Delta H_v$ and $h\Delta T$, so they can be considered negligible compared with the other terms. Therefore, Eqs. (3) may be written

$$\begin{aligned} h_1 (T_1 - T_2) &= N\Delta H_v + \frac{k_m}{\delta} (T_2 - T_3) \\ h_1 (T_1 - T_2) &= h_2 (T_3 - T_4) \end{aligned} \tag{5}$$

The temperatures calculated with Eqs. (3) and Eqs. (5) differ very little under our experimental conditions.

MARCEL DEKKER, INC.
270 Madison Avenue, New York, New York 10016

From the last two equations we get

$$\Delta T_{\mathrm{m}} \equiv T_2 - T_3 = \frac{\Delta T_{\mathrm{b}} - \dfrac{N\Delta H_{\mathrm{v}}}{h}}{1 + \dfrac{k_{\mathrm{m}}}{\delta h}} \tag{6}$$

where $\Delta T_{\mathrm{b}} = T_1 - T_4$ and

$$\frac{1}{h} = \frac{1}{h_1} + \frac{1}{h_2} \tag{7}$$

The temperature polarization coefficient, τ, is the fraction of the total thermal driving force, ΔT_{b}, used to generate the mass transfer driving force, ΔT_{m}. Ideally, the temperature polarization coefficient should be close to unity. It is defined as follows:

$$\frac{\Delta T_{\mathrm{m}}}{\Delta T_{\mathrm{b}}} = \frac{T_2 - T_3}{T_1 - T_4} = \tau \tag{8}$$

Mass Transfer Equations

Mass transfer is driven by the vapor pressure difference of the solution on either side of the membrane. The mass flux density N may be written as

$$N = C\,(P_{\mathrm{w}2} - P_{\mathrm{w}3}) \tag{9}$$

where C is a mass transfer coefficient for the system, whose form depends on the model used to describe the transport mechanism (7, 8). Resistance to mass transfer comes from both the membrane structure and the possible presence of air trapped inside the membrane pores. Resistance due to the membrane structure (in the absence of air) may be described by the Knudsen diffusion model, by surface diffusion, and/or by the Poisseuille flux model. Resistance due to air trapped inside the membrane may be described by the gas stagnant film diffusion model and by the thermal diffusion model.

As the interfacial pressures cannot be directly measured, they must be expressed as a function of temperature. If we restrict the study to dilute solutions (assuming that the pressure on the feed side of the membrane is equal to the saturation pressure of pure water at the temperature of the membrane surface; in any case, an estimation of the difference in pressures when the correction due to the presence of a solute is considered is at most of the order of 3%), to small ranges of temperature (because in the Taylor expansion of ΔP, any ΔT terms of second order and higher are considered negligible), and if we use the

Clausius–Clapeyron equation for $(dP^*_w/dT)_m$, substitution from Eq. (6) into Eq. (9) gives

$$\frac{\Delta T_b}{N\Delta H_v} = \frac{1}{C}\left(1 + \frac{k_m}{\delta h}\right)\left(\frac{1}{\Delta H_v\left(\frac{dP^*_w}{dT}\right)_m}\right) + \frac{1}{h} \tag{10}$$

where P^*_w is the water vapor equilibrium pressure, and dP^*_w/dT must be evaluated at the mean temperature between T_2 and T_3. This equation, formerly obtained by Schofield et al. (9), may be used for analysis of the experimental results. Therefore, a graph of $\Delta T_b/N\Delta H_v$ plotted against $1/\Delta H_v(dP^*_w/dT)_m$ should yield a straight line with a slope equal to $(1/C)(1 + k_m/\delta h)$ and an intercept $1/h$, assuming that the thermal conductivity and thickness of the membrane can be estimated. The h_i $(i = 1, 2)$ coefficients are known by assuming that the Nusselt number is given by the empirical correlation due to Sieder and Tate for dimensionless numbers (10):

$$\mathrm{Nu} = \frac{hD}{k} = 1.86\left(\mathrm{Re}\cdot\mathrm{Pr}\cdot\frac{D}{L}\right)^{1/3}\left(\frac{\mu}{\mu_s}\right)^{0.14} \tag{11}$$

where Nu, Re, and Pr are the Nusselt, Reynolds, and Prandt numbers, respectively; D is the equivalent diameter of the flow channel (11); k is the thermal conductivity; L is the tube length; and μ is the viscosity. In Eq. (11) the fluid properties are evaluated at the bulk solution temperature except for the quantity μ_s, which is the dynamic viscosity and is evaluated at the temperature of the channel surface.

Equation (11) is an empirical correlation for short tubes and forced convection, i.e., for tubes shorter than the thermal and velocity entry lengths in laminar flow (combined entry length). This correlation has been recommended for values of $(\mathrm{Re}\cdot\mathrm{Pr}/L/D)^{1/3}$ $(\mu/\mu_s)^{0.14} \geq 2$, uniform T, and $0.48 < \mathrm{Pr} < 16{,}700$, $0.044 < (\mu/\mu_s) < 9.75$.

Under our experimental conditions the above criteria are satisfied, so Eq. (11) is suitable using the hydraulic diameter for our duct, at least to a first approximation.

From the definition of h in Eq. (7), the following equation is obtained:

$$\frac{1}{h} = \frac{1}{h_1}\left(1 + \frac{h_1}{h_2}\right) \tag{12}$$

since h in this expression is known from the fit to Eq. (10), and by estimating h_1/h_2 (assuming that both are given by the correlation in Eq. 11), it is possible to estimate h_1, h_2, and the constant of proportionality in Eq. (11) for our

experimental device. In our device the cells are not symmetrical (see Experimental Section), and the linear velocity through the cell on the cold side is different from that on the warm side, so h_1 and h_2 cannot be assumed to be equal.

Similarly, the following empirical correlation was given by McAdams (12) as suitable in laminar flow for fully developed hydrodynamic conditions (parabolic velocity profile) and for values of $Wc_p/KL > 10$:

$$\frac{hD}{k} = 1.75\left(\frac{Wc_p}{kL}\right)^{1/3} \tag{13}$$

where W is the mass flow, c_p is the specific heat at constant pressure, and the other quantities have been defined. This correlation is not suitable for our use because the parabolic velocity profile has not been determined. However, it can be used for comparison with the Sieder and Tate correlation. As in the previous case, the constant of proportionality in this correlation can also be determined for our device from Eq. (12).

Gas Stagnant Film Diffusion Model

Once the temperatures at the liquid–vapor interfaces are known, it is possible to calculate the theoretical fluxes by using the gas stagnant film diffusion model (13). Udriot (14), who compared values of the C coefficient obtained for membranes of the same material but with different pore sizes, found that the values were practically the same for all the membranes. This suggests that vapor transfer through a membrane is by ordinary or continuous diffusion, since this is the only mechanism in which, theoretically, C is not dependent on pore size. In this model the molar flux density through the membrane may be written as

$$N_m = \left(\frac{PD_{ef}}{RT_m\delta}\right)\ln\frac{1-x_{A3}}{1-x_{A2}} = \left(\frac{PD_{ef}}{RT_m\delta}\right)\ln\frac{P-P_{A3}}{P-P_{A2}} \tag{14}$$

where N_m is the molar flux density; P is the total pressure; R is the gas constant; T_m is the average thermodynamic temperature; δ is the membrane thickness; x_{A2}, x_{A3}, P_{A2}, and P_{A3} are the water vapor mole fractions and partial pressures at the first and second ends of the pore, respectively; and D_{ef} is the effective diffusion coefficient, defined as

$$D_{ef} = \frac{D_{AB}\varepsilon}{\chi} \tag{15}$$

where D_{AB} is the diffusion coefficient of the water vapor–air mixture, ϵ is the void volume fraction, and χ is the membrane tortuosity factor.

EXPERIMENTAL

The experimental setup in a vertical configuration is shown in Fig. 2. The solutions were contained in two controlled temperature double-wall reservoirs. These solutions were circulated by two variable flow peristaltic pumps. Two flowmeters were used for continuous recording of the flow rate through the cell. A digital pressure gauge registered the pressure at the feed entry into the cell. Heat exchangers between the thermostats and the reservoirs improved the temperature control. Temperatures were measured in the cell, in the frame, and in the cooling plates using Pt-100 thermometers.

The feeds were aqueous solutions of sucrose, glucose, or fructose. Distilled water was used on the cold side except where another indication is given. The membranes were made of 0.20 μm PTFE with PP support (PTS20) (supplied by Gore), and of 0.45 μm PVDF (PV45) (supplied by Millipore).

Experiments were made using direct contact membrane distillation with the cell placed upright, as in Fig. 2, with two membranes at either side of the frame, as well as with the cell placed horizontally and with a single membrane. Two different cells were used for measurements in the vertical configuration

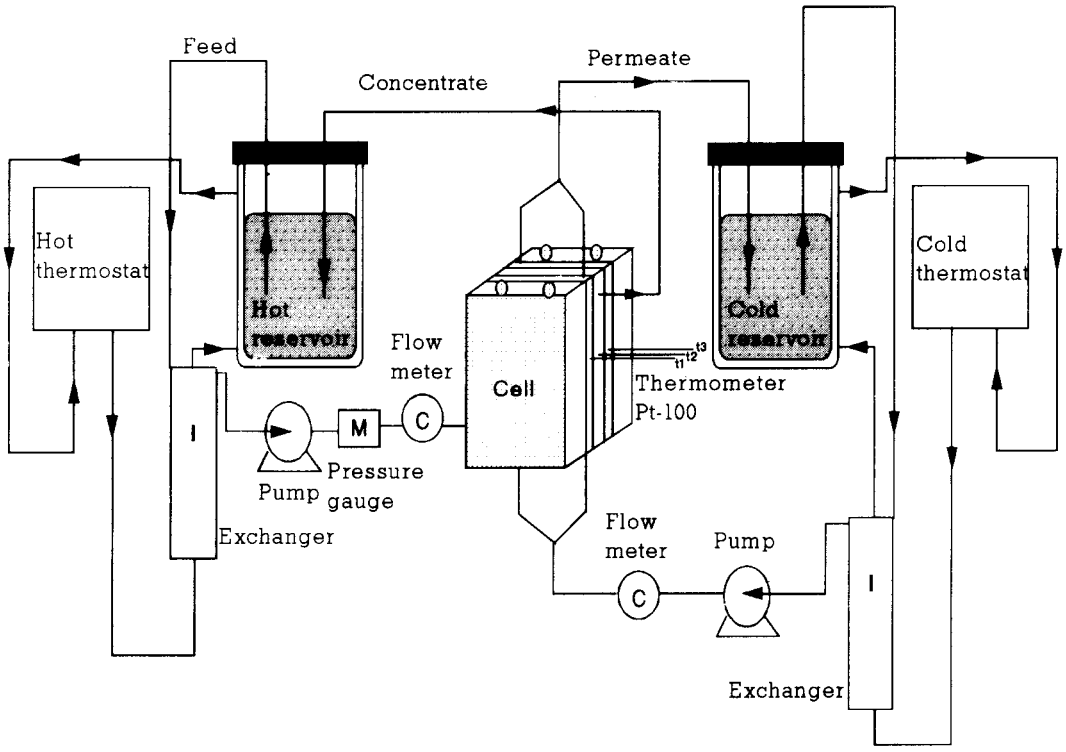

FIG. 2 Schematic representation of membrane distillation apparatus at vertical configuration. Membrane dimensions: length = 11.958×10^{-2} m and width = 5.964×10^{-2} m. Two membranes.

MARCEL DEKKER, INC.
270 Madison Avenue, New York, New York 10016

with two membranes in parallel, one made of brass and the other of stainless steel. A third cell, a Minitan-S tangential flow filtration (TFF) system from Millipore, was used in the horizontal configuration. In the latter case, only one membrane was employed. The flow through the cell was always tangential to the membrane, and the flow through the membrane was determined from the temporal evolution of the liquid level in the reservoirs. The cell dimensions were approximately $(13 \times 7) \times 10^{-2}$ m. In the case of the stainless steel and brass cells, the thicknesses of both feed cell frames were 0.7×10^{-2} m, and the thicknesses of permeate cell frames at the cold side were 1.1×10^{-2} m in the case of the stainless steel cell and $<1 \times 10^{-3}$ m in the case of the brass cell.

In our work conditions the flow rate through the feed zone was twice the flow rate through each permeate zone (see Fig. 2). In addition, the liquid thicknesses on both sides of the membranes were different (so the cross sections were different and the linear velocities on both sides were also different). Therefore the cells were not physically symmetrical.

RESULTS AND DISCUSSION

Membrane Properties

Membrane Void Volume Fraction

The method used to estimate the void volume fraction is described in Ref. 15. It can be measured by making use of a pycnometer, a balance, isopropyl alcohol (IPA), and water. In this method use is made of the fact that IPA penetrates into the pores of the membrane and water does not penetrate into the pores of the membrane.

The void volume fraction may be estimated from the polymer material density and the membrane density by the following equation:

$$\varepsilon = 1 - \frac{\rho_m}{\rho_{pol}} \tag{16}$$

The ε values obtained experimentally together with their standard errors are shown in Table 1 for each type of membrane.

TABLE 1
Void Volume Fraction (ε), Thickness (δ), Liquid Entry Pressure of Water (LEP_w), and Thermal Conductivity (k_m) for the Membranes Used

Membrane	ε	δ (μm)	LEP_w (bar)	k_m (W/m·K)
PV45	66 ($\pm$ 2)	116 ($\pm$ 9)	1.10 ($\pm$ 0.04)	0.040 $\pm$ 0.009
PTS20	44 ($\pm$ 6)	184 ($\pm$ 8)	4.63 ($\pm$ 0.01)	0.043 $\pm$ 0.007

Membrane Thickness

The membrane thickness was measured with a micrometer, Millitron-Compact Measuring Instrument, Model 1202 IC; the accuracy varied depending on the scale chosen. In order to avoid membrane deformation due to the pressure exerted by the probe, a razor was set over the membrane. The razor thickness was measured and subtracted from the total thickness to determine the membrane thickness. Measurements were made at many points on the membrane surface.

The δ values obtained and their standards errors are shown in Table 1.

Liquid Entry Pressure of Water (LEP_W)

The liquid entry pressure of water is the pressure that must be applied to pure water before it will penetrate into a nonwetted (dry) membrane. The following procedure, described in Ref. 16, was used for the determination of the LEP_W. The apparatus for this measurement is shown in Fig. 3. The membrane was set on a holder. The pressure exerted on the membrane was slowly increased until a continuous flow in the capillary was achieved. At that moment the pressure value was read, and that value was used as the LEP_W. In Table 1 the LEP_W values are shown together with their standard deviations.

Thermal Conductivity

Thermal conductivity of membranes was measured by making use of a modification of the Lees method as described in Ref. 16. The results obtained together with their errors are shown in Table 1.

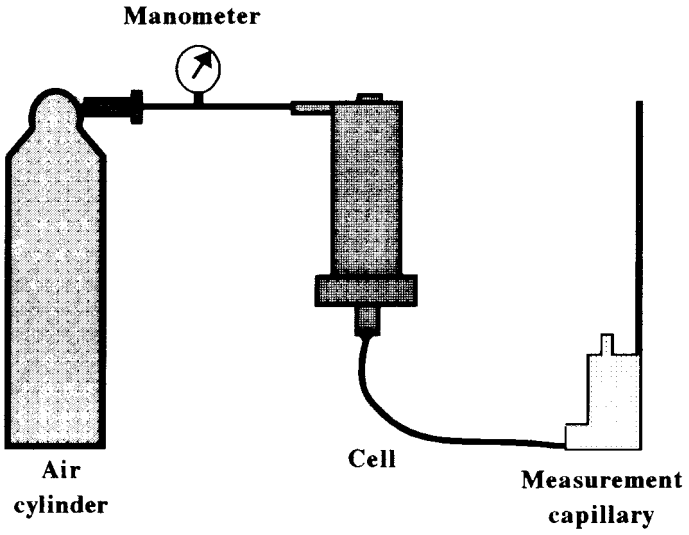

FIG. 3 Schematic representation of the apparatus for the determination of the liquid entry pressure.

MARCEL DEKKER, INC.
270 Madison Avenue, New York, New York 10016

Solution Properties

Viscosity of Aqueous Sucrose Solutions

Viscosity measurements were made using a Lauda Viscotimer S/2 and a DMA 55 densimeter. Sucrose aqueous solutions with different concentrations were prepared. The densimeter was calibrated at 20°C. In the beginning the operating temperature was chosen, then the density was measured and the sample was put into the viscometer. It was necessary to delay measuring the viscosity until the system was thermostable, and the apparatus gave us the time involved. From the time (t^*), the solution density (ρ), and the calibration constants, the viscosity (μ) was calculated using the following equation:

$$\frac{\mu t^*}{\rho} = At^{*2} - \mathrm{B} \tag{17}$$

in which A and B are the calibration constants. Later the operating temperature was changed to 25, 35, 45, and 52°C. Figure 4 shows the dependence of the viscosity with concentration for the different temperatures, and their values at 20°C (17).

The viscosity was fitted versus the concentration by means of the equation

$$\mu = \alpha \exp(-\beta c) \tag{18}$$

where c is the concentration expressed in weight percent of solute, and α and β are the fit coefficients. In all cases the correlation coefficient was greater than 0.99 for four measuring points. The fit coefficients with their standard errors are shown in Table 2. It can be seen from Fig. 4 and Table 2 that the viscosity increases exponentially with the solute concentration and decreases with the temperature.

Density of Aqueous Sugar Solutions

Solution density was measured with a DMA 58 densimeter which allowed us to know the density to five decimal figures. The densimeter was calibrated at 20°C using two standards supplied by the manufacturer, A. Paar. One of

TABLE 2
Estimates of the Regression Parameters (together with their standard errors) of the Viscosity Fit to an Exponential Function of the Concentration (Eq. 18), for Different Temperatures of Sucrose Aqueous Solutions

Coefficient	t = 25°C	t = 35°C	t = 45°C	t = 52°C
α (10^{-3} kg/m·s)	0.45 (± 0.10)	0.39 (± 0.09)	0.37 (± 0.06)	0.35 (± 0.05)
β	0.061 (± 0.006)	0.057 (± 0.005)	0.051 (± 0.004)	0.048(± 0.004)

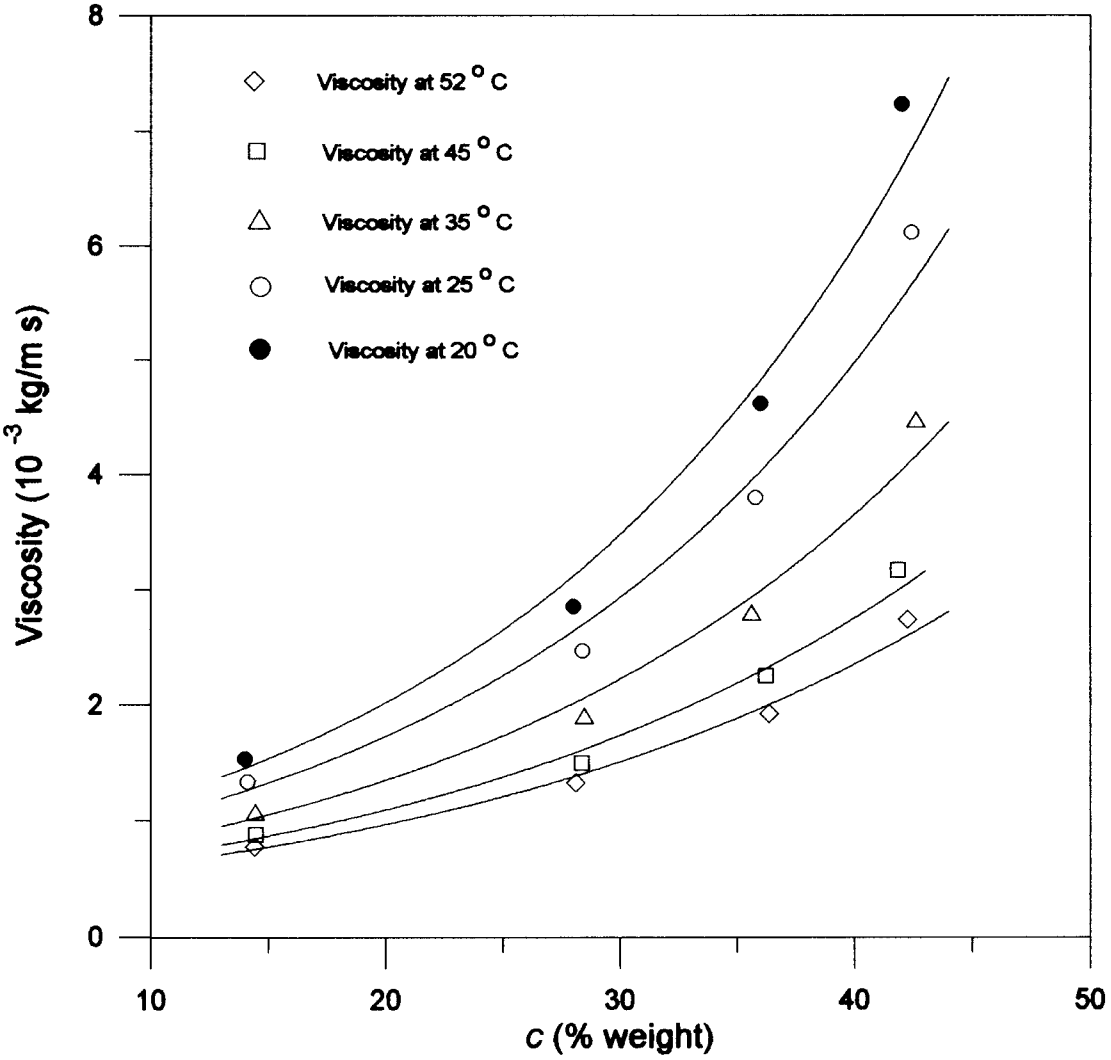

FIG. 4 Dependence of the viscosity with the concentration of sucrose aqueous solutions at different temperatures. The solid lines are the fits to Eq. (18).

them was tetrachloroethylene with $\rho = 1.623$ g/cm^3 at 20°C and a 5–50°C temperature range, and the other was a lubricating oil (nominal 30 cSt at 40°C) with $\rho = 0.874$ g/cm^3 at 15°C and the same temperature range. Glucose, fructose, and sucrose aqueous solutions were prepared and their densities were measured. The operating temperature was successively changed to 30, 40, and 50°C, and all the calibration process procedures were repeated. Figure 5 shows the dependence of the density on the concentration (expressed in weight percent of solute) at each temperature for sucrose solutions. The dependence was very similar with the other solutions; in all cases it was linear with the concentration and the correlation coefficient was greater than 0.99 for

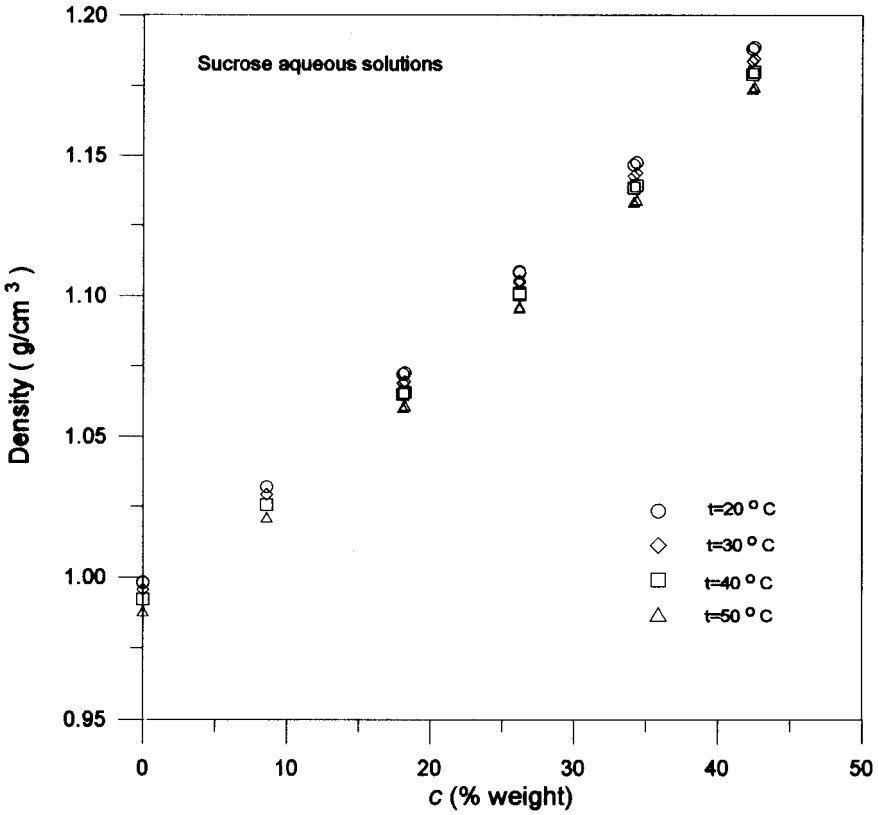

FIG. 5 Density as a function of the sucrose aqueous solutions concentration at different temperatures.

twelve measuring points. It was observed that in all cases the density decreases when the temperature increases.

Experimental Results and Discussion

The effects of different parameters on the mass flow results are as follows.

Flow Rate through the Cell

Tests were made at different flow rates through the upright stainless steel cell and two membranes (0.20 μm PTFE with PP support). The tests lasted about 8 hours and the distillate flow was approximately constant. The plot in Fig. 6 shows the linear increase of the distillate volume flow with the flow rate through the cell which is because the effects of concentration and temperature polarizations decrease when the flow rate through the cell increases. The solid line is the best linear fit of the data.

MARCEL DEKKER, INC.
270 Madison Avenue, New York, New York 10016

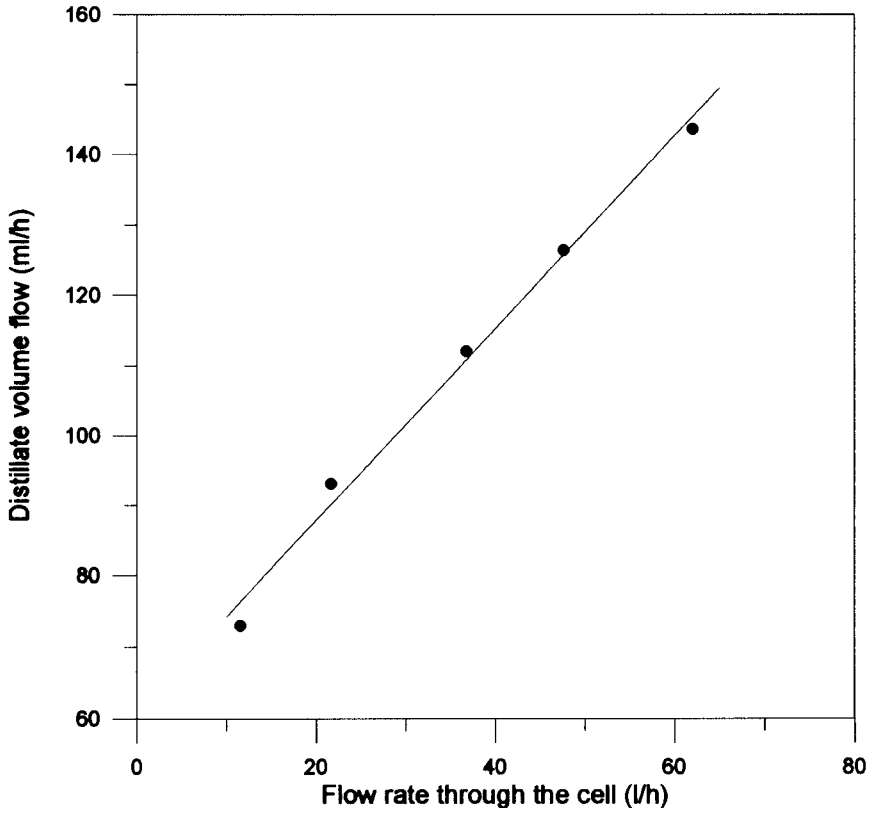

FIG. 6 Distillate volume flow versus feed flow rate through the cell. PTS20 membranes. Feed initial concentration of sucrose: 150 g/L. Stainless steel cfell. $t_f = 47.5°C$, $t_c = 22.5°C$. The solid line is the linear fit of the experimental data.

Nature of the Feed Solution

Experiments were made with aqueous solutions of sucrose, glucose, and fructose, using the Minitan-S TFF system in the horizontal configuration at the maximum speed of the peristaltic pumps (flow rate through the cell = 66 L/h). The results were practically identical, as shown in Fig. 7, which shows the temporal evolution overlapping of the feed solution refractive indices. It is observed that the feed concentration rate (curve slope) increases quickly with the time.

Initial Concentration of the Feed Solution

Tests were carried out with different initial concentrations of the aqueous sucrose solution using the upright stainless steel cell. The experimental distillate volumes have been fitted to a quadratic function of time in Fig. 8. The quadratic form is more marked as the feed initial

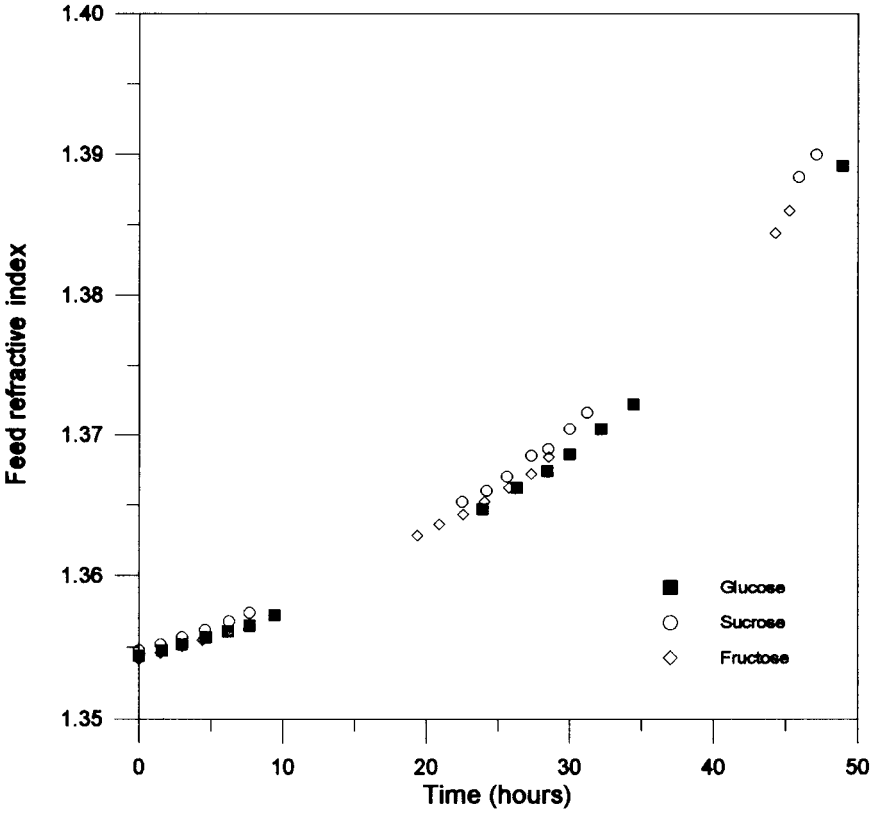

FIG. 7 Feed refractive index versus time for aqueous solutions of glucose, sucrose, and fructose. Feed initial concentration: 150 g/L. Flow rate through the cell tangential to the membrane: 66 L/h. PV45 membrane. Minitan-S system in horizontal position, $t_f = 22.5°C$, $t_c = 9.5°C$.

concentration increases. As a consequence, the distillate flows calculated from $V(t^*)$ are linear with time during the experimental period, increasing, for each time value, as the initial concentration decreases. Figure 9 shows the linear decrease of the average distillate flow with the initial concentration of the feed solution. This result is to be expected because of the decrease of the water vapor pressure due to the greater presence of solute.

The feed concentration temporal evolution has been fitted to a quadratic function in Fig. 10. The slope of the concentration as a function of time, dc/dt^*, shows a linear dependence. In the initial time its value increases as the feed initial concentration increases. For initial concentrations of 75, 150, 225, 300, and 375 g/L the slope of the straight line $dc/dt^* = a + bt^*$ is positive whereas for an initial concentration of 450 g/L it is negative. Larger values of dc/dt^* are obtained for 225 g/L than for

MARCEL DEKKER, INC.
270 Madison Avenue, New York, New York 10016

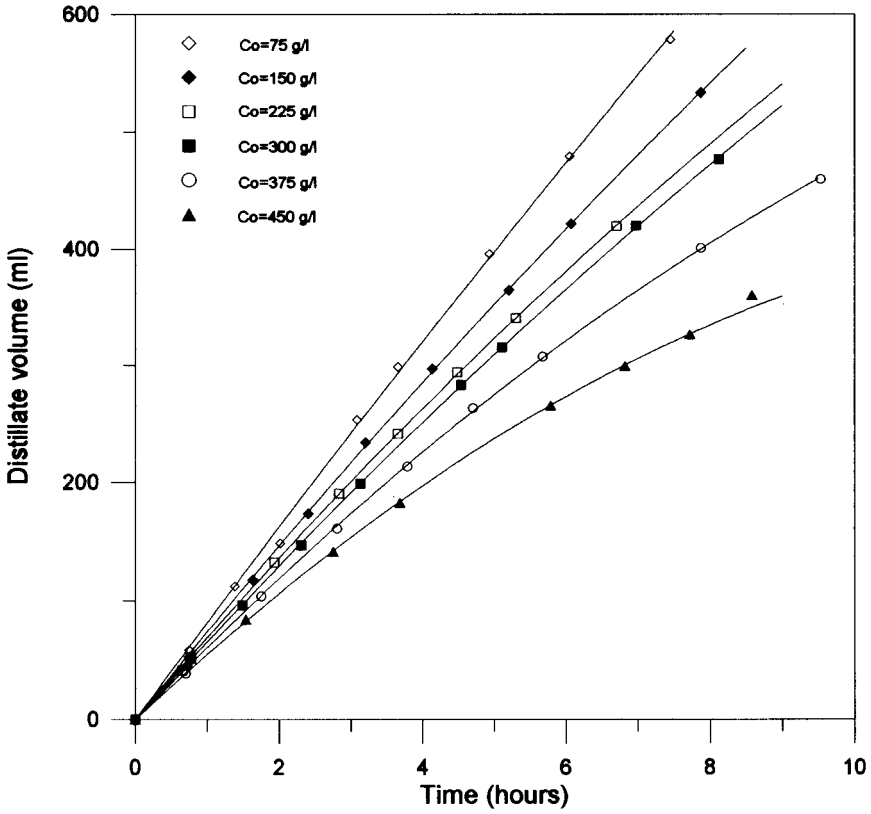

FIG. 8 Temporal evolution of the distillate volume for different initial concentrations. PTS20 membranes. Aqueous solutions of glucose. Flow rate through the cell: 46.5 L/h. Stainless steel cell, $t_f = 47.5°C$, $t_c = 22.5°C$. The solid line is the fit of the experimental data to a quadratic function.

150 g/L, and for 150 g/L greater than for 75 g/L for every time. However, for initial concentrations greater than 225 g/L those straight lines cross and therefore the former behavior is no longer valid.

In Fig. 10 the points corresponding to the same distillate volume (V) or which are equivalent to the same hot reservoir volume are shown. These points are on quadratic functions whose form is accentuated as time increases. It is clearly observed that the time necessary to obtain the same distillate volume increases when the initial concentration increases.

Changes of the concentration with time, dc/dt^*, corresponding to points of the same distillate volume or which are equivalent of the same hot reservoir volume show a maximum that is initially slightly lower than 375 g/L for a distillate volume of 150 mL and that is later displaced to lower initial concentration values, so that when the distillate volume is 350 mL, it is situated at a slightly lower value than 300 g/L.

MARCEL DEKKER, INC.
270 Madison Avenue, New York, New York 10016

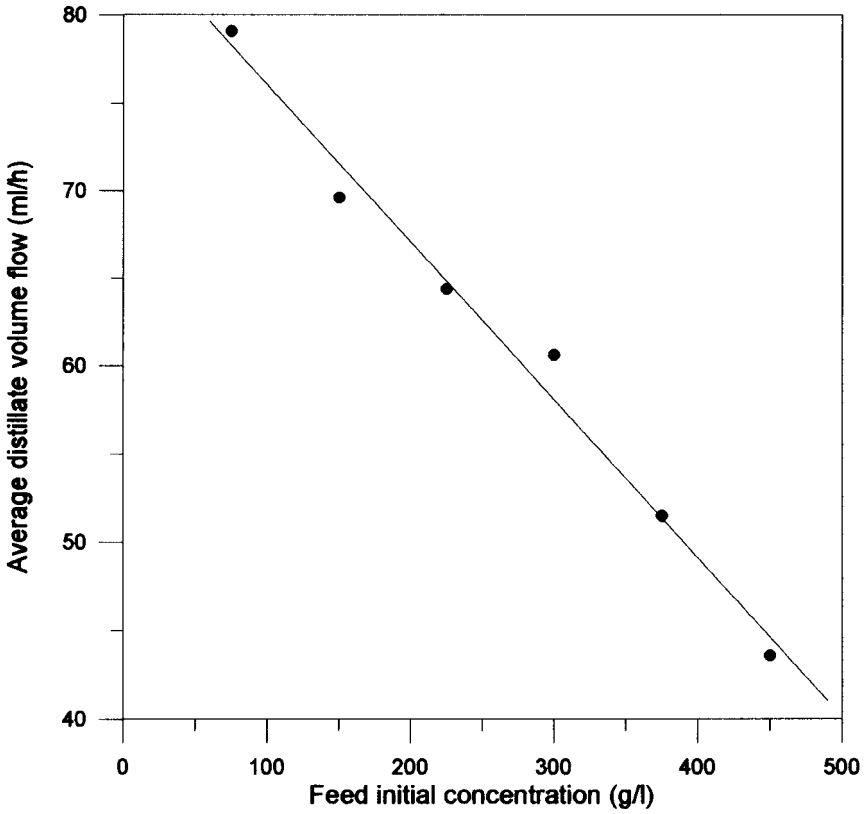

FIG. 9 Distillate volume flow versus feed initial concentration. PTS20 membranes. Aqueous solutions of glucose. Flow rate through the cell: 46.5 L/h. Stainless steel cell, $t_f = 47.5°C$, $t_c = 22.5°C$. The solid line is the linear fit of the experimental data.

Temperature Differences and Mean Temperatures

In the first set of experiments T_m was varied while maintaining ΔT constant. In the second set ΔT was varied while maintaining T_m constant. PTS20 membranes and two types of cells (upright stainless steel and brass) were used. The feeds were sucrose aqueous solutions ($C_0 = 150$ g/L). The experimental data obtained were fitted to Eq. (10), which provided the coefficients h and C as presented in Table 3.

Then tests were run with PV45 membranes and with the upright brass cell. The mean temperature was kept constant and the temperature difference was varied, which excluded any fit of the experimental data to Eq. (10) since the independent variable remained constant.

Experiments with the Stainless Steel Cell and PTS20 Membranes. In these experiments the mean temperature was kept constant and

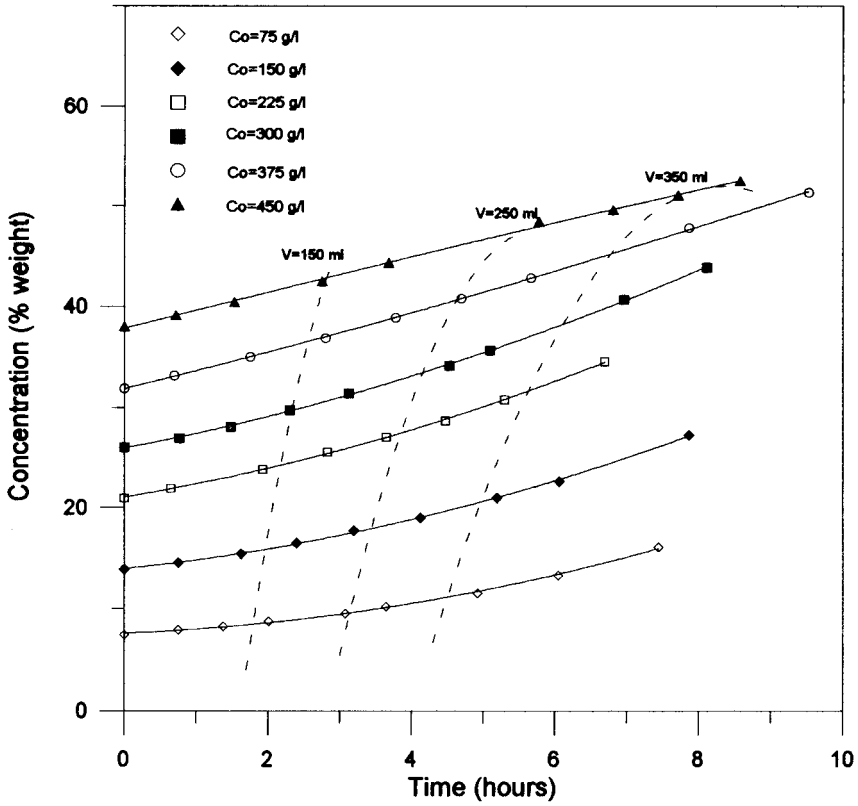

FIG. 10 Temporal evolution of the feed concentration (weight percent of solute). The dashed lines are the quadratic curves of the points corresponding to the same distillate volume. PTS20 membranes. Aqueous solutions of glucose. Flow rate through the cell: 46.5 L/h. Stainless steel cell, $t_f = 47.5°C$, $t_c = 22.5°C$. The solid lines are the fits of the experimental data to a quadratic function.

the temperature difference was varied. Figure 11 shows the influence of these externally applied differences on the distillate volume flow for each mean temperature, which is seen to be a linear increase with ΔT, an obvious result because this is the driving force in the process. When the temperature differ-

TABLE 3
Fit Coefficients to Eq. (10). PTS20 Membranes. Measurements of Mass Flux Systematically Changing ΔT and T_m. Feed Initial Concentration: 150 g/L

Cell	$1/h$ ($m^2 \cdot K/W$)	$(1 + k_m/\delta h)/C$ ($m^2 \cdot s \cdot Pa/kg$)	C ($kg/m^2 \cdot s \cdot Pa$)	h ($W/m^2 \cdot K$)
Brass	$1.38 (\pm 0.14) \times 10^{-3}$	$9.6 (\pm 0.9) \times 10^{5}$	$13.8 (\pm 1.5) \times 10^{-7}$	$720 (\pm 80)$
Stainless steel	$1.98 (\pm 0.23) \times 10^{-3}$	$16.3 (\pm 1.1) \times 10^{5}$	$9.0 (\pm 0.6) \times 10^{-7}$	$510 (\pm 60)$

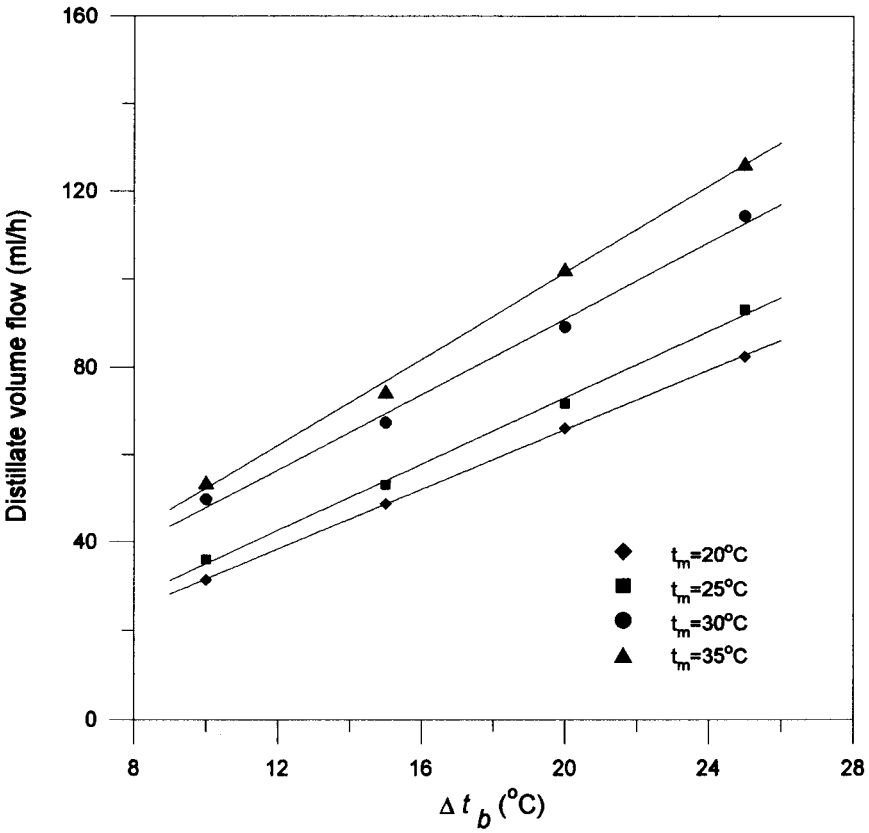

FIG. 11 Influence of Δt_b in the distillate volume flow for different t_m. Aqueous solutions of sucrose, feed initial concentration: 150 g/L. PTS20 membranes. Stainless steel cell. Flow rate through the cell: 47 L/h. The solid lines are the linear fits of the experimental data.

ence was kept constant, the dependence on the mean temperature was found to be exponential. The initial feed concentration was 150 g/L and the flow rate through the cell was 47 L/h. The experimental data were fitted to Eq. (10), and from the global transfer coefficient h, the h_1 and h_2 coefficients and the proportionality constant in Eq. (13) for our device, 3.4, were estimated, and from these coefficients an estimation was made of the temperature profile using Eqs. (3). The experimental fluxes were then fitted to Eq. (14), which gave the effective diffusion coefficient, D_{ef}, which was 0.203 ($\pm$0.010) $\times 10^{-4}$ m^2/s. By using Eqs. (5) and (14) the effective diffusion coefficient was determined; its value, 0.202 ($\pm$0.010) $\times 10^{-4}$ m^2/s, was almost identical to the previously found value. This proves that the terms $Nc_p\Delta T$ can be considered negligible compared with the other terms in Eqs. (3). The correlation in Eq. (11), with the proportionality constant for our device, 4.4, was also used to calculate the heat transfer coefficients, and with Eqs. (5) the temperatures and the temperature

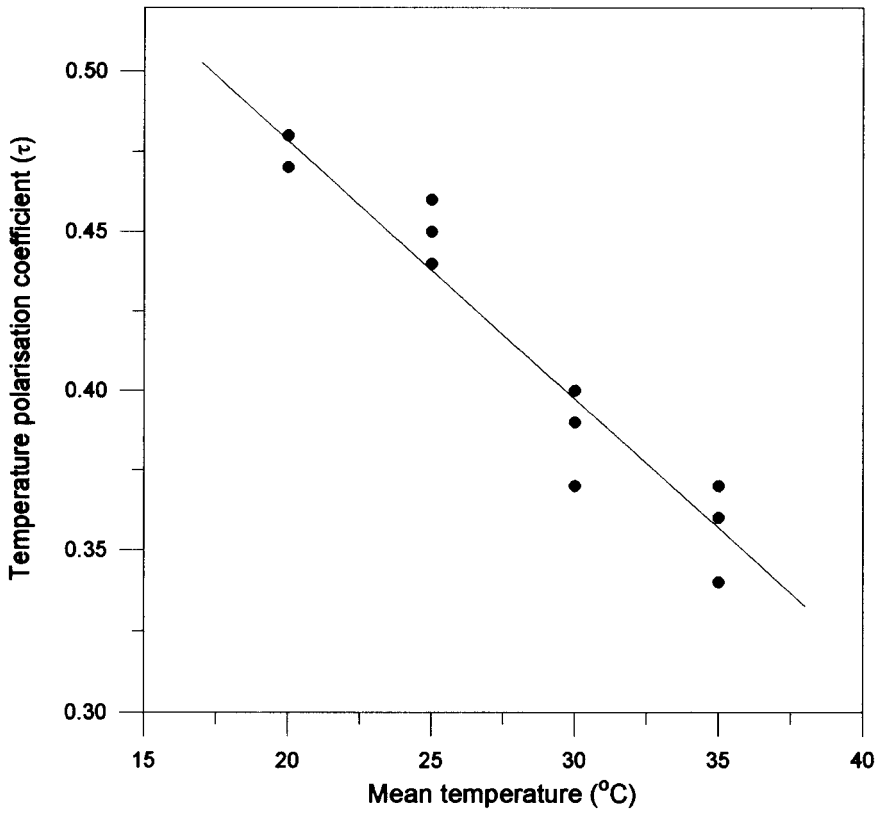

FIG. 12 Influence of mean temperature in the temperature polarization coefficient estimated using the correlation in Eq. (11), constant of proportionality: 4.4 and Eqs. (5). Stainless steel cell. PTS20 membranes. Flow rate through the cell: 47 L/h. Aqueous solutions of sucrose, feed initial concentration: 150 g/L. The solid line is the linear fit of the experimental data. The dispersion in ordinates corresponds to different temperature differences (ΔT).

polarization coefficient τ were calculated. The latter is shown in Fig. 12 as a function of the bulk solution average temperature. In this figure it can be seen that τ decreases linearly with T_m. The dispersion in ordinates corresponds to different temperature differences (ΔT). Finally, the experimental fluxes were fitted to Eq. (14) and the results obtained are given in Table 4.

From the effective diffusion coefficient, the diffusion coefficient of the water vapor–air mixture, D_{AB}, was calculated by using the experimental value of the porosity and assuming $\chi = 1.5$. Our D_{AB} values, given in Table 4, are larger than those given in the literature (18), 0.27×10^{-4} m^2/s.

The correlation coefficients of the two fits to Eq. (14) (using Eqs. 13 and 11, respectively, together with Eqs. 5 for the temperature profile) were, respectively, 0.9967 and 0.9964 for sixteen points. The coefficients h_1 and h_2, shown in Table 4, are seen to be practically the same in the two correlations, which is also true for the effective diffusion coefficient, D_{ef}. The small differences

TABLE 4
Heat Transfer Coefficients h_1 and h_2, Effective Diffusion Coefficient D_{ef}, and Diffusion Coefficient of the Mixture D_{AB}, Together with Their Standard Errors, Obtained with the PTS20 Membranes, Using Eqs. (5) for the Temperature Profile and with the Stainless Steel Cell. Feed Initial Concentration: 150 g/L. Flow Rate through the Cell: 47 L/h

Correlation	Proportionality constant	h_1 ($W/m^2 \cdot K$)	h_2 ($W/m^2 \cdot K$)	D_{ef} (m^2/s)	D_{AB} (m^2/s)
Eq. (11)	4.4 (this work)	1300	830	$0.206 (\pm 0.010) \times 10^{-4}$	$0.70 (\pm 0.10) \times 10^{-4}$
Eq. (13)	3.4 (this work)	1400	800	$0.202 (\pm 0.010) \times 10^{-4}$	$0.69 (\pm 0.10) \times 10^{-4}$

between them are included within the experimental errors. In the case of the correlation of Eq. (11) and the proportionality constant 4.4, the theoretical flux densities were estimated by the gas stagnant film diffusion model and compared in Fig. 13 with the experimental flux densities. Nearly all the points are on the bisectrix of the first quadrant, which shows that the model reproduces

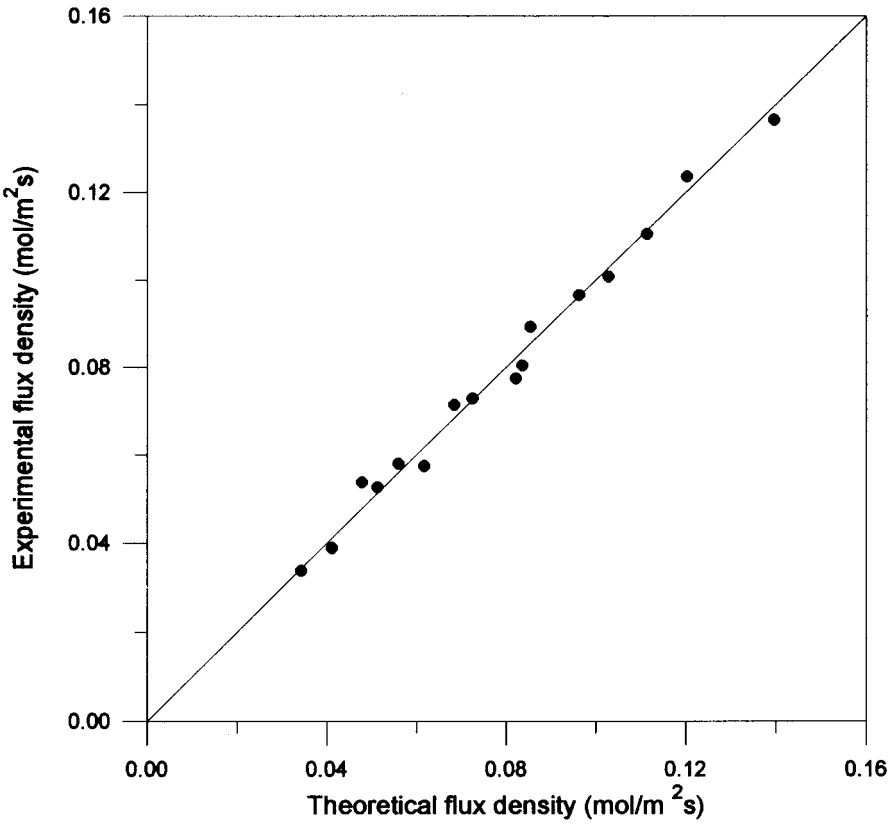

FIG. 13 Experimental molar flux density versus theoretical molar flux density (Eq. 14). The correlation of Eq. (11) with the proportionality constant 4.4 was used. PTS20 membranes. Stainless steel cell.

reasonably well the experimental fluxes, but with high values of D_{AB}. This may be because the membrane is a composite of the polypropylene support and the PTFE film, and therefore the definitions of the void volume fraction and of the membrane tortuosity may not be very precise.

In Fig. 14 the molar flux density versus the interfacial water vapor pressure difference is shown. In this case the correlations in Eq. (13) and Eqs. (5) for the temperature profile are used. These experimental data were also fitted to Eq. (9), with $R^2 = 0.9967$ for sixteen points, which showed that under our conditions of measurement the mass transfer coefficient C is practically a constant within the range of temperatures studied.

Experiments with the Brass Cell and PTS20 Membranes. Exactly the same procedure was followed with the upright brass cell, but in this case the temperature difference was fixed and the mean temperature was changed from one experiment to another. That is to say, at $\Delta T = 5°C$ the mean temperature was varied from 20 to 35°C; at $\Delta T = 10°C$ from 25 to 40°C; at $\Delta T = 15°C$ from 25 to 40°C; and at $\Delta T = 20°C$ from 30 to 45°C, in 5°C intervals. The feed initial concentration was 150 g/L and the flow rate through

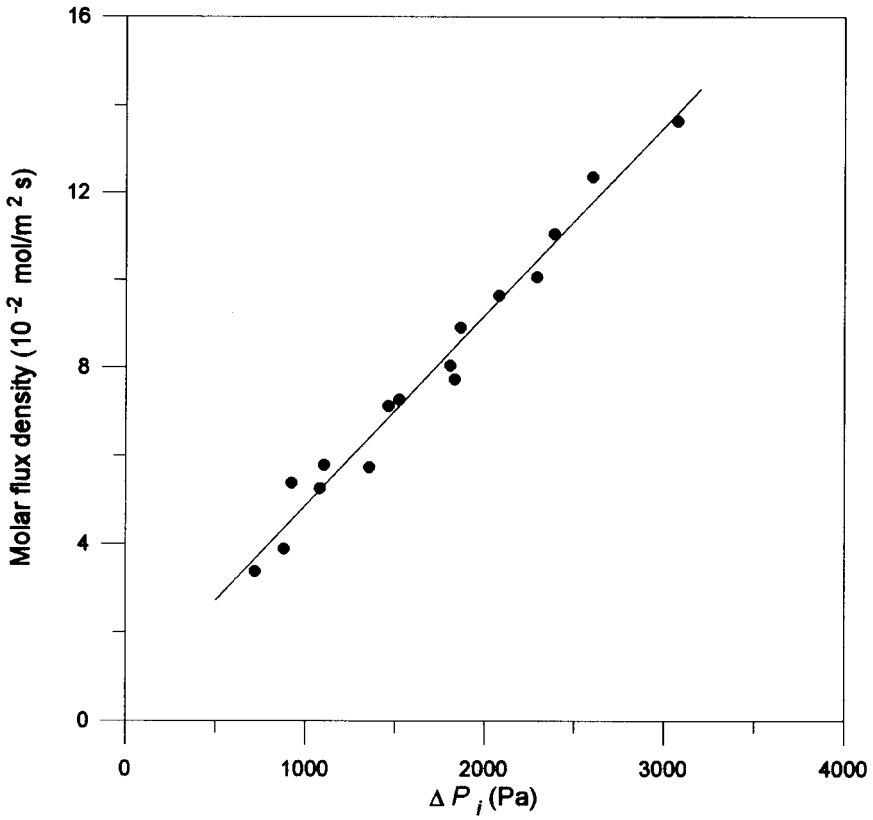

FIG. 14 Molar flux density versus interfacial vapor pressure difference. The correlation of Eq. (13) was used. PTS20 membranes. Stainless steel cell.

MARCEL DEKKER, INC.
270 Madison Avenue, New York, New York 10016

the cell was 44 L/h. The experimental data were fitted to Eq. (10) as shown in Fig. 15, where the observed dispersion in ordinates corresponds to different temperature differences (ΔT). The proportionality constants h_1 and h_2 for our system were obtained from the global heat transfer coefficient h by using the correlations given by Eqs. (11) and (13). From the heat transfer coefficients and the other parameters such as ΔH_v, k_m, etc., an estimation was made of the liquid–vapor interface temperatures using Eqs. (5), and from these latter the water vapor pressures were found. The experimental fluxes were fitted to Eq. (14) of the gas stagnant film diffusion model. The results are shown in Table 5. In this case the coefficient h_2 varied considerably with the correlation used, although the values of D_{ef} showed only a small change. An important point here is that with the brass cell the thickness of water in the cold side was too small to ensure a constant temperature. The correlation coefficients, R^2, were 0.9776 and 0.9740, respectively, for sixteen points, which shows that the fits were good, although the D_{AB} values were high compared to literature values.

Experiments with the Brass Cell and PV45 Membranes. Experiments were also made with PV45 membranes and with the brass cell placed

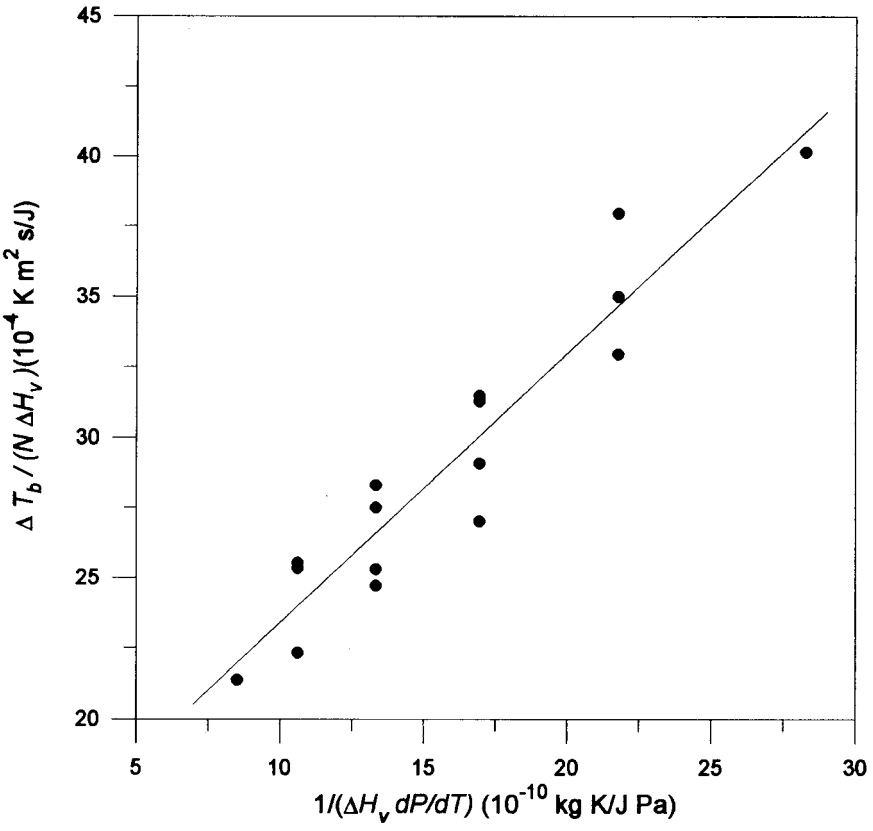

FIG. 15 Fit of the data to Eq. (10). Aqueous solutions of sucrose, initial concentration: 150 g/L. Flow rate through the cell: 44 L/h. PTS20 membranes. Brass cell.

TABLE 5
Heat Transfer Coefficients h_1 and h_2, and Effective Diffusion Coefficient D_{ef}, Together with Its Standard Error, Obtained with the PTS20 Membranes, Using the Brass Cell. Feed Initial Concentration: 150 g/L. Flow Rate through the Cell: 44 L/h.

Correlation	Proportionality constant	h_1 (W/m^2·K)	h_2 (W/m^2·K)	D_{ef} (m^2/s)
Eq. (11)	3 (this work)	860	4501	$0.42\ (\pm\ 0.03) \times 10^{-4}$
Eq. (13)	2 (this work)	780	9400	$0.43\ (\pm\ 0.03) \times 10^{-4}$

vertically at constant mean temperature, which excluded any fit of the experimental data to Eq. (10). Aqueous sucrose solutions were circulated on both sides of the membrane. C_{0f} = 98.5 g/L and C_{0c} = 313 g/L. The flow rate through the cell was 47 L/h. Figure 16 shows the influence of the applied tem-

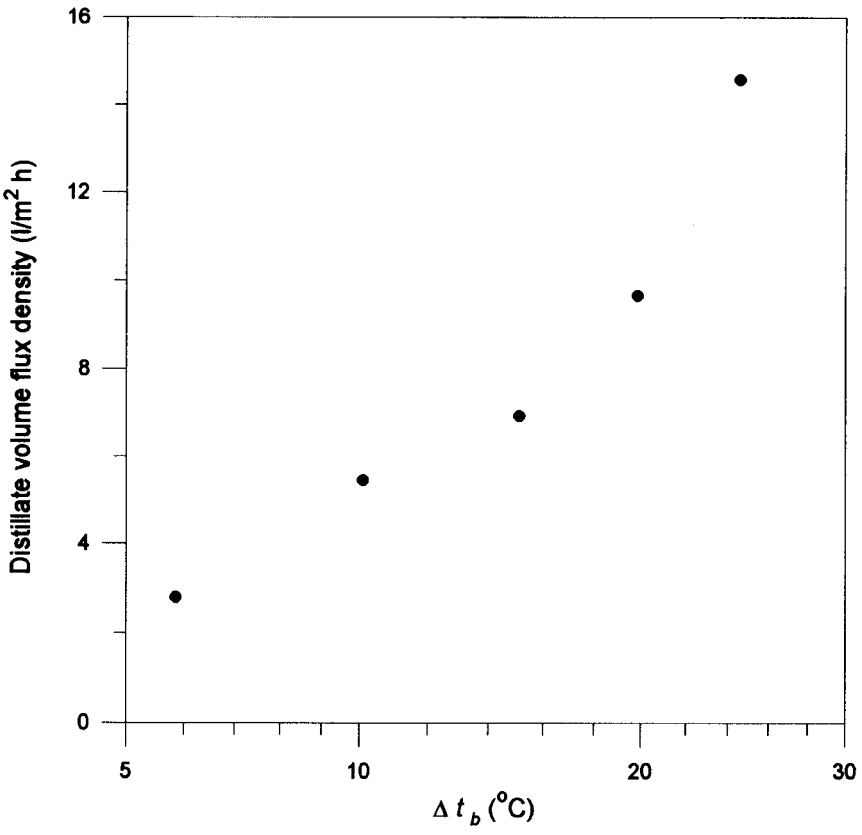

FIG. 16 Influence of bulk temperature difference, Δt_b, on density of the distillate volume flux. Sucrose aqueous solutions at both sides. C_{of} = 98.5 g/L, C_{oc} = 313 g/L. Flow rate through the cell: 47 L/h. PV45 membranes. Brass cell, t_m = 32.2°C.

MARCEL DEKKER, INC.
270 Madison Avenue, New York, New York 10016

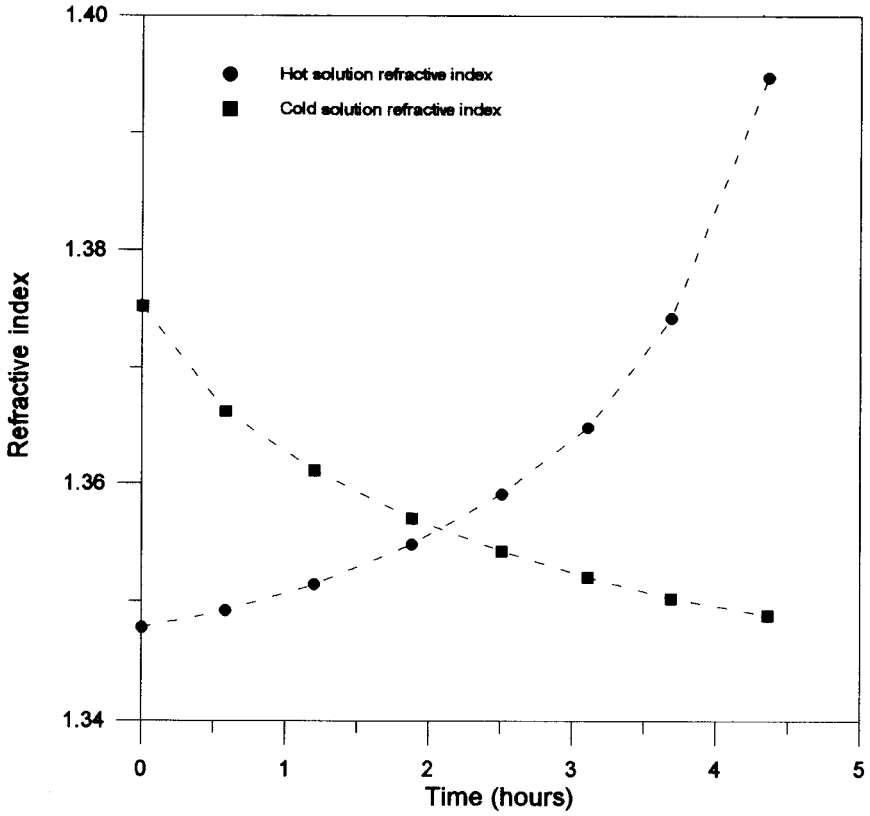

FIG. 17 Hot and cold solutions refractive indices versus time. Sucrose aqueous solutions at both sides. $C_{of} = 98.5$ g/L, $C_{0c} = 313$ g/L. Flow rate through the cell: 47 L/h. PV45 membranes. Brass cell, $t_f = 44.7°C$, $t_c = 20.1°C$.

perature difference on the distillate flux density. The observed dependence is clearly not linear. Figure 17 shows the temporal evolution of the refractive indices of the two solutions for the case of the experiment with a larger ΔT. In this figure it is observed that the concentration rate at the feed side is greater than the dilution rate at the cold side. The h_1 and h_2 coefficients were calculated using Eq. (13) with its proportionality constant 1.75, and with that obtained previously for the brass cell, 2, as well as using Eq. (11) with the constant obtained for this cell (see Table 5), 3. From the h_1 and h_2 heat transfer coefficients and other parameters, an estimation was made of the liquid–vapor interface temperatures using Eqs. (5), and from these latter the interfacial water vapor pressures. The experimental flux data were fitted to the gas stagnant film diffusion model. The results obtained are shown in Table 6. The h_2 values are seen to vary considerably with the correlation used in each case. The effective diffusion coefficients, D_{ef}, remain practically constant; their differences are included within the experimental errors. Here again, the D_{AB} values are higher than those tabulated.

TABLE 6
Heat Transfer Coefficients h_1 and h_2, and Effective Diffusion Coefficient D_{ef}, Together with Its Standard Error, Obtained with the PV45 Membranes, Using the Brass Cell. $C_{0_f} = 98.5$ g/L and $C_{0_c} = 313$ g/L. Flow Rate through the Cell: 47 L/h

Correlation	Proportionality constant	h_1 (W/m^2·K)	h_2 (W/m^2·K)	D_{ef} (m^2/s)
Eq. (11)	3 (this work)	890	4,300	$0.29\ (\pm 0.05) \times 10^{-4}$
Eq. (13)	1.75	740	10,900	$0.34\ (\pm 0.06) \times 10^{-4}$
	2 (this work)	840	12,300	$0.29\ (\pm 0.04) \times 10^{-4}$

CONCLUSIONS

The influence of several parameters on membrane distillation was investigated and the following findings were made:

1. The distillate volume flow increases linearly with the flow rate through the cell.
2. There is no difference between the results obtained in the temporal evolution of the refractive indices using aqueous solutions of sucrose, glucose, and fructose with the same initial concentration.
3. The average distillate volume flow decreases linearly with the feed initial concentration. The experimental distillate volumes have been fitted to a quadratic function of time, the concentration temporal evolution also has been fitted to a quadratic function, and the changes of the concentration with time corresponding to the points with the same distillate volume show a maximum that is displaced to lower values of the initial concentration when the distillate volume is increased.
4. It was found that at a fixed mean temperature the flow showed a linear dependence with the temperature difference, and that for each temperature difference the dependence of the flow with the mean temperature was exponential.

Several systems of equations are proposed, generalizing those in the literature, to estimate the interfacial temperatures in direct contact membrane distillation. Analysis of the data shows that the results obtained with Eqs. (3) are practically identical to those provided by the simpler Eqs. (5). For this reason the latter were employed in most cases. A linear fit of the experimental data provides not only the coefficient of global heat transfer, h, but also that of mass transfer, C. In the range of temperatures investigated, this coefficient is practically a constant.

The gas stagnant film diffusion model reproduces the experimental data reasonably well, but requires higher diffusion coefficient values, D_{AB}, than the tabulated ones.

One of the main error source in an analysis of the results is the estimation of the heat transfer coefficients because of their implications in the evaluations of the evaporation and condensation temperatures. Also, some approximations were performed in obtaining Eq. (10); for example, that k_m is approximately constant for each experiment, that terms of the form $Nc_p\Delta T$ are negligible compared to other terms, that terms of second order and higher are negligible in the Taylor expansion of ΔP in terms of ΔT. So it is possible that some of these approximations may influence on the determination of h and C coefficients and the results that follow.

SYMBOLS

A	calibration constant (cm^2/s^2)
B	calibration constant (cm^2)
c	concentration (weight percent of solute)
C	mass transfer coefficient ($kg/m^2 \cdot s \cdot Pa$)
C_0	initial concentration (g/L)
C_0^*	Nc_p ($J/m^2 \cdot s \cdot K$)
c_p	specific heat at constant pressure ($J/kg \cdot K$)
D	tube diameter (m)
D_{AB}	diffusion coefficient of the mixture (m^2/s)
D_{ef}	effective diffusion coefficient (m^2/s)
h	film heat transfer coefficient ($W/m^2 \cdot K$)
ΔH_v	evaporation enthalpy (J/kg)
k	thermal conductivity ($W/m \cdot K$)
L	tube length (m)
M	molar mass (kg/mol)
N	mass flux density ($kg/m^2 \cdot s$)
N_m	molar flux density ($mol/m^2 \cdot s$)
Nu	Nusselt number (—)
ΔP	pressure difference (Pa)
P	total pressure (Pa)
P_0^*	pure water vapor pressure (Pa)
Pr	Prandtl number (—)
$q_{H\text{-}I}$	total enthalpy flux in the left side ($J/m^2 \cdot s$)
R	gas constant ($J/mol \cdot K$)
Re	Reynolds number (—)
t^*	time (h)
t	temperature (°C)

MARCEL DEKKER, INC.
270 Madison Avenue, New York, New York 10016

T	temperature (K)
T_m	mean temperature (K)
ΔT	temperature difference (K)
W	mass flow (kg/s)
x	mole fraction (—)
y_l	fluid film thickness (m)

Greek Letters

α	fit coefficient (kg/m·s)
β	fit coefficient
δ	membrane thickness (m)
ε	membrane porosity (void volume fraction) (—)
χ	membrane tortuosity (—)
μ	viscosity (kg/m·s)
ρ	density (kg/m^3)
τ	temperature polarization coefficient (—)

Subscripts

1,2,3,4	defined in Fig. 1
A,w	water vapor
b	bulk
c	cold
f	feed
gas	gas
i	interfacial
l	liquid
m	membrane
matrix	membrane matrix
pol	polymer
0	reference
s	surface
v	vapor

ACKNOWLEDGMENTS

The authors thank CICYT (Spain), Projects ALI-91-1126-CO3-02 and ALI-94-1044-CO3-02, for the financial support accorded to this investigation.

REFERENCES

1. E. Drioli, Y. Wu, and V. Calabro, "Membrane Distillation in the Treatment of Aqueous Solutions," *J. Membr. Sci.*, *33*, 277–284 (1985).

2. R. W. Schofield, A. G. Fane, C. J. D. Fell, and R. Macoun, "Factors Affecting Flux in Membrane Distillation," *Desalination*, *77*, 279–297 (1990).
3. M. A. Izquierdo-Gil, "Separación de disoluciones acuosas de azúcares mediante membranas porosas hidrófobas y gradientes de temperatura" ("Separation of Sugar Aqueous Solutions Using Hydrophobic Porous Membranes and Temperature Differences"), Ph.D. Thesis, University Complutense of Madrid, 1997.
4. K. W. Lawson and R. Lloyd, "Review: Membrane Distillation," *J. Membr. Sci.*, *124*, 1–25 (1997).
5. A. P. Colburn and T. B. Drew, "The Condensation of Mixed Vapors," *Trans. AIChE*, *33*, 197 (1937).
6. T. K. Sherwood, R. L. Pigford, and C. R. Wilke, *Mass Transfer*, McGraw-Hill, New York, NY, 1975.
7. R. W. Schofield, A. G. Fane, and C. J. D. Fell, "Gas and Vapour Transport through Microporous Membranes: I. Knudsen–Poseuille Transition," *J. Membr. Sci.*, *53*, 159–172 (1990).
8. R. W. Schofield, A. G. Fane, and C. J. D. Fell, "Gas and Vapour Transport through Microporous Membranes: II. Membrane Distillation," *Ibid.*, *53*, 173–185 (1990).
9. R. W. Schofield, A. G. Fane, and C. J. D. Fell, "Heat and Mass Transfer in Membrane Distillation," *Ibid.*, *33*, 299–313 (1987).
10. A. J. Chapman, *Heat Transfer*, 3rd ed., Macmillan, New York, NY, 1974.
11. A. Bejan, *Convection Heat Transfer*, Wiley, New York, NY, 1984.
12. W. H. McAdams, *Heat Transmission*, 3rd ed., McGraw-Hill, New York, NY, 1954.
13. R. B. Bird, W. E. Stewart, and E. N. Lightfoot, *Transport Phenomena*, Wiley, New York, NY, 1976.
14. H. Udriot, "Distillation Transmembranaire—Etude d'un procédé de séparation a membrane et développement de nouveaux champs d'application," Ph.D. Thesis, Swiss Federal Institute of Technology. Lausanne, 1990.
15. K. Smolder and A. D. M. Franken, "Terminology for Membrane Distillation," *Desalination*, *72*, 249–262 (1989).
16. M. C. García-Payo, "Destilación en membranas de disoluciones acuosas de alcoholes" ("Membrane Distillation of Alcohols Aqueous Solutions"), Ph.D. Thesis, University Complutense of Madrid, 1998.
17. *Handbook of Chemistry and Physics*, 55th ed., CRC Press, 1974–1975.
18. E. N. Fuller, K. Ensley, and J. C. Giddings, "Diffusion of Halogenated Hydrocarbons in Helium. The Effect of Structure on Collision Cross Sections," *J. Phys. Chem.*, *73*, 3679–3685 (1969).

Received by editor May 1, 1998
Revision received October 1998

PAGE 1802 IS BLANK

MARCEL DEKKER, INC.
270 Madison Avenue, New York, New York 10016

Request Permission or Order Reprints Instantly!